A Rigorous Model for Spaceborne Linear Array Sensors

Daniela Poli

Abstract

A rigorous sensor model for the georeferencing of imagery from CCD linear array sensors with along-track stereo viewing is presented. The model is based on the classical collinearity equations, which are extended for the specific characteristics of the acquisition of CCD linear scanners. It includes the sensor position and attitude modeling with second-order piecewise polynomials depending on the acquisition time and a self-calibration for the correction of radial and decentering lens distortions, principal point(s) displacement, focal length(s) variation and CCD line(s) rotation in the focal plane. Using well-distributed GCPs and, additionally, Tie Points (TPs), the external orientation and self-calibration parameters, together with the TPs ground coordinates, are estimated in a least-square adjustment. In order to demonstrate the flexibility of the model, stereo images from pushbroom sensors with different characteristics have been oriented with sub-pixel accuracy in the checkpoints. The results are presented and discussed.

Introduction

Linear array sensors for Earth observations are widely used for the acquisition of imagery in pushbroom mode from spaceborne and on airborne platforms. They offer panchromatic and multispectral images with spatial resolution ranging from few centimeters (airborne sensors) up to thousands of meters (spaceborne sensors). Images provided by these sensors have very high potential for photogrammetric mapping at different scales and for remote sensing applications. For example, they can be used for the generation of Digital Elevation Models (DEM), that represent an important basis for the creation of Geographic Information Systems, and the production of 3D texture models for visualization and animation purposes (Grün *et al.*, 2004).

In the classical photogrammetric chain that starts with the radiometric preprocessing of the raw images and goes to the generation of products like the DEMs, the orientation of the images is a fundamental step, and its accuracy is a crucial issue during the evaluation of the entire system. For pushbroom sensors, the triangulation and photogrammetric point determination are rather different compared to standard approaches, which are usually applied for full frame imagery, and require special investigation of the sensor geometry and the acquisition mode. Moreover, pushbroom scanners in use show different geometric characteristics (optical systems, number of CCD lines, scanning mode, and stereoscopy), and for each data set, specific information is available (ephemeris, GPS/INS observations, calibration, and other internal parameters).

For the georeferencing of imagery acquired by pushbroom sensors, geometric models with different complexity, rigor, and accuracy have been developed as described for example in Fritsch and Stallmann (2000), Hattori *et al.* (2000), Dowman and Michalis (2003), and Toutin, (2004b). In most cases, rigorous models such as Rational Polynomial Models (RPM), Direct Linear Transformations (DLT), and affine projections are used. In this paper we will focus on rigorous models. These models try to describe the physical properties of the image acquisition. While in frame photogrammetry each image is geometrically described by a central perspective, images acquired by pushbroom sensors are the result of a perspective projection in each line and parallel projection between lines. Using rigorous models, the collinearity equations have to be extended in order to include the external (and eventually internal) orientation modeling. The differences between the proposed rigorous models exist in the internal and external orientation modeling and their flexibility; some rigorous models are designed for specific sensors, while others are more general and can be used for different sensors. Few models are designed for both spaceborne and airborne linear scanners.

As an example, in the software SPOTCHECK+ (Kratky, 1989), the satellite position is derived from known nominal orbit relations, while the attitude variations are modeled by a simple polynomial function (linear or quadratic). For self-calibration, two additional parameters are added: the focal and the principle point correction. This model has been used for the orientation of SPOT (Baltsavias and Stallmann, 1992), MOMS-02/D2 (Baltsavias and Stallamann, 1996), and MOMS-2P (Poli *et al.*, 2000). An advantage of this software is that it can easily integrate new pushbroom instruments, if the corresponding orbit and sensor parameters are known. The model was also investigated and extended in (Fritsch and Stallmann, 2000). At the Chair of Photogrammetry and Remote Sensing at the Technical University of Munich, the existing block adjustment program CLIC has been extended for the photogrammetric point determination of airborne and spaceborne three-line scanners (Ebner *et al.*, 1992). For the external orientation, a polynomial approach with orbital constraints in case of spaceborne imagery is utilized. In the airborne case the exterior orientation parameters are estimated only for so-called orientation points at certain time intervals and in between, the parameters of each third image-line are expressed as polynomial functions (e.g., Lagrange polynomials) of the parameters at the neighboring orientation points. If differential GPS and INS measurements are imported, systematic errors of the position and attitude observations are modeled through additional strip- or block-invariant parameters for each exterior orientation function.

CyberCity AG, Inder Luberzen 3, CH 8902, Urdorf, Switzerland (dpoli@cybercity.tv).

Photogrammetric Engineering & Remote Sensing
Vol. 73, No. 2, February 2007, pp. 187–196.

0099-1112/07/7302–0187/$3.00/0

The model was tested on MOMS-02/D2 and 2P (Ebner *et al.*, 1992), MEOSS (Ohlhof, 1995), HRSC and WAOSS (Ohlhof and Kornus, 1994) sensors. The same model has been adopted at DLR for the geometric in-flight calibration and orientation of MOMS-2P imagery (Kornus *et al.*, 1999).

The University College London (UCL) suggested a dynamic orbital parameter model (Gugan and Dowman, 1988). The satellite movement along the path is described by *two-orbital* which are modeled with linear angular changes with time. The attitude variations are described by drift rates. This model was successfully applied for SPOT level 1A and 1B, MOMS-02 and IRS-1C (Valadan *et al.*, 1999) imagery. In (Dowman and Michalis, 2003), this approach was investigated and extended for the development of a general sensor model for along-track pushbroom sensors. The results obtained with SPOT-5/HRS are reported in (Michalis and Dowman, 2004).

The IPI Institute in Hannover has developed the program BLASPO for the adjustment of satellite line scanner images (Konecny *et al.*, 1987). Only the general information about the satellite orbit together with the view directions in-track and across-track are required. Six exterior orientation parameters represent the uniform motion, and eight additional parameters describe the difference between the approximate uniform movement and the reality. Systematic effects caused by low frequency motions are handled by self calibration with additional parameters This program seems very flexible, because it has been used for the orientation of different pushbroom sensors carried on satellite, like MOMS-02 (Büyüksalih and Jacobsen, 2000), SPOT and IRS-1C (Jacobsen *et al.*, 1999), Ikonos and QuickBird (Jacobsen and Passini, 2003), SPOT5-5/HRS (Jacobsen, 2004) and on airborne sensors, such as DPA (Jacobsen and Passini, 2003).

Another flexible and rigorous model for pushbroom sensors has been developed by Toutin (Toutin, 2004a) and embedded in PCI Geomatica®. The model takes into account the distortions relative to the platforms, to the sensor, to the Earth, and the cartographic projection.

In other models, such as in Westin (1990), the orbital model used is simpler than in the previous models. A circular orbit instead of elliptical orbit is used. Using SPOT data, seven unknown parameters need to be computed for each image.

At the Institute of Geodesy and Photogrammetry, ETH Zurich, a rigorous model has been developed for the georeferencing of pushbroom sensors carried on spaceborne and airborne platforms. The main requirement was to be as flexible as possible and adaptable to a wide class of linear array sensors, but still being based on rigorous photogrammetric formulations. The main characteristics of the model and the approach used are presented. For testing, the model has been applied on sensors with different characteristics (multi-line and single-line sensors at different ground resolution with synchronous and asynchronous acquisition modes) carried on satellites and airborne platforms. The results achieved with the three line sensor StarImager® by Starlabo, Tokyo have been already reported in (Poli, 2002). In this paper, we will concentrate on satellite applications and present the results achieved with MOMS-2P, SPOT-5/HRS, and the ASTER-VNIR sensors.

Sensor Model

Each image acquired by CCD linear array sensors consists of lines independently acquired at different times and with a different sensor external orientation (position and attitude). Today, geopositioning systems provide the direct measurement of the sensor position and attitude at specific instants of time, then, accurate interpolation techniques allow the calculation of the corresponding data at any time and for each image line. Furthermore, the satellite trajectories can be predicted or simulated by using the physical properties of the satellite orbits. This information, together with suitable interpolating techniques, may be used to calculate the sensor position and attitude for the particular instants of acquisition and apply a direct georeferencing. Otherwise, an indirect georeferencing approach based on a bundle adjustment is required.

Our sensor model includes both approaches. According to the availability of information on the sensor internal and external orientation, the direct or the indirect georeferencing methods are used. The methods are described in the following paragraphs.

Direct Georeferencing

The principle of direct georeferencing is to estimate the ground coordinates of the homologous points measured in the images through a forward intersection using as internal orientation, the results of laboratory calibrations; and as external orientation, the data provided by the geopositioning systems carried on the platform, or the trajectory, calculated by mathematical formulas (only for satellite-based sensors). This approach does not require any ground control points, except for final checking, and does not estimate any additional parameters modeling the interior and exterior orientation. For this reason, the effectiveness and reliability of this method depend on the accuracy of the internal and external orientation data.

In the case of airborne pushbroom sensors the use of GPS and INS systems is essential for the georeferencing of the imagery. In fact, with these sensors, a bundle adjustment is unrealistic, because the number of unknown external orientation parameters (six for each image line) would be too large. Moreover, the aircraft trajectory cannot be predicted and modeled, as in the satellite case. Therefore, the direct measurement of the sensor position and attitude is indispensable.

For the imagery acquired by pushbroom sensors carried on a satellite, the sensor external orientation can be computed from the physical properties of the orbits, through the Keplerian elements, or from the state vectors contained in the ephemeris. The position and orientation of a satellite along its orbit in the ECI system can be calculated using the Keplerian parameters. The assumption is that the satellite is subjected to the gravitational force only and no perturbations occur. Depending on the image metadata format, the state vectors can be available. In general, a state vector is a set of position, velocity and attitude values for a particular time. The number of state vectors, the time interval between the observations and the reference systems used are varying from a space agency to the other.

The position, velocity and attitude are usually measured with instruments carried on board. Star trackers, for example, take an image of a region of the sky using a CCD-like optical camera, and compare successive images to determine how much the orientation of the satellite has drifted. This information is used by the spacecraft pointing system to determine the actual pointing direction of the satellite at any instant. In other satellites, this information is sent to an attitude control system which then corrects for the drift by using on-board thrusters or other motion-generating devices to maintain the correct satellite pointing (Image, 2005). The position and velocity vectors in the satellite ephemeris are used to calculate the external orientation of the camera with respect to the Earth Centered Inertial (ECI) the Earth Centered Fixed (ECR) coordinate systems. The difference between the two frames is that ECI is an inertial system, therefore, it does not rotate with respect to the Earth and is fixed with respect to the celestial frame.

On the other hand, the ECR is fixed with respect to the Earth frame and is synchronized with the Earth's rotation. In both systems the *X*- and *Y*- axes lay on the Equatorial plane and *Z* is directed along the Earth rotation axis, but in case of ECI system *X* is directed toward the vernal equinox (fixed in the celestial frame), while in case of ECR system *X* is directed toward the Greenwich meridian (solid for the Earth's rotation). The transformation between ECI and ECR frames is a rotation around the *Z*-axis depending on time; the angle is computed through physical well-known formulas (Seidelmann *et al.*, 1992).

The time of acquisition of each line is calculated with a linear interpolation using the time of acquisition of a line of reference and the integration time, that is, the time required by the optical system to scan one line on the ground. For the interpolation of the position and attitude, cubic splines are used.

If available, the internal orientation is the result of a pre-flight or an in-flight calibration. The parameter definition varies with the space agency. For example, in case of SPOT-5/HRG and SPOT-5/HRS the viewing directions of each pixels is given; for ASTER also the same information is given but only for a limited number of so-called lattice points. In case of airborne sensors, such as the ADS40 or StarImager®, the position of each pixel in the focal plane is given.

Using the sensor external orientation estimated for each line and any internal orientation parameters available from laboratory calibration, the image coordinates of homologous points are transformed in the object system through a forward intersection (direct georeferencing). Like in frame photogrammetry, the points are measured in the image and transformed from image to camera system, through an affine transformation and from camera to object system, based on the collinearity equations. Then, the object coordinates are estimated with forward intersection in two steps. In the first one, the approximation of the ground coordinates are calculated by intersecting the two most external images, because the base over height ratio is larger, and the stereoscopy is more favorable. Once the approximate ground coordinates are known, they are refined with a least squares solution in the second step, using all the available lines. The relationship between camera and ground (or object) coordinates is described by the collinearity equations:

$$\begin{bmatrix} X \\ Y \\ Z \end{bmatrix} = \begin{bmatrix} X_C \\ Y_C \\ Z_C \end{bmatrix} + mR(\omega_C,\varphi_C,\kappa_C) \begin{bmatrix} x - x_0 \\ y - y_0 \\ -f \end{bmatrix} \tag{1}$$

where $[X, Y, Z]$ are the point coordinates in the ground system, $[X_C, Y_C, Z_C]$ is the PC position in the ground system, $[x, y]$: point coordinates in the camera system; $[x_0, y_0]$ are the principal point coordinates in the camera system; f is the focal length, m is the scale factor and $R(\omega_C,\varphi_C,\kappa_C)$ represents the rotation matrix from camera to ground system. The object system used for the georeferencing is the local tangential system for airborne sensors and the ECR systems for spaceborne sensors.

For the evaluation of the accuracy of the method a sufficient number of Check Points (CPs) is required. The CPs are measured in the images and in the object space. After applying the direct georeferencing, the estimated ground coordinates of the CPs are compared to the correct ones and the RMSE are calculated.For the orientation of pushbroom imagery, the approach based on direct georeferencing is very powerful because it allows the determination of the ground coordinates of the points measured in the images without the use of Ground Control Points (GCPs), with a considerable reduction of the processing time, costs, and efforts. It is a very useful tool for the evaluation of the accuracy that can be achieved in the object space using only the information provided by laboratory calibration and positioning systems carried on aircraft or spacecraft. For example, the algorithm has been used for the determination of the ground coordinates of points measured in Meteosat scenes (Seiz *et al.*, 2004).

Indirect Georeferencing

The indirect georeferencing model is a bundle adjustment for the estimation of the correct sensor external and internal orientation. It is used if the interior or the exterior orientation measurements are not suitable for high precision mapping with direct georeferencing. According to this approach, the collinearity equations are extended in order to included: multi-lens sensors, the external orientation modeling, the integration of any available GPS/INS, and the systematic errors due to the lens and CCD lines.

For sensors whose optical systems consist of more lenses, additional geometric parameters describing the relative position and attitude of each lens with respect to the nadir one are imported in the collinearity equations. For each lens j, d_{xj}, d_{yj}, d_{zj} represent the relative position and α_j, β_j, γ_j, the relative attitude with respect to the reference one.

The sensor external orientation is modeled by Piecewise Polynomial Functions (PPM) depending on time. Due to the possibility of changing the number of segments and the polynomial degree, this function produces quite flexible results and is applicable to both satellite and airplanes trajectories (Hofmann *et al.*, 1982; Kratky, 1989; Valadan-Zoej and Foomani, 1999; Grün and Zhang, 2002). If one segment only is used, a parabolic function is obtained. According to the PPM approach, the platform trajectory is divided into segments and in each segment i, with time extremes t^i_{ini} and t^i_{fin}, the variable $\bar{t}$ is defined as:

$$\bar{t} = \frac{t - t^i_{ini}}{t^i_{fin} - t^i_{ini}} \in [0,1] \tag{2}$$

where t is the time of acquisition of a generic image line.

Then, in each segment the sensor external orientation $[X_C, Y_C, Z_C, \omega_C, \varphi_C, \kappa_C]$ is modeled with second-order polynomials depending on $\bar{t}$:

$$\begin{aligned} X_C(\bar{t}) &= X^i_0 + X^i_1\bar{t} + X^i_2\bar{t}^2 \\ Y_C(\bar{t}) &= Y^i_0 + Y^i_1\bar{t} + Y^i_2\bar{t}^2 \\ Z_C(\bar{t}) &= Z^i_0 + Z^i_1\bar{t} + Z^i_2\bar{t}^2 \\ \omega_C(\bar{t}) &= \omega^i_0 + \omega^i_1\bar{t} + \omega^i_2\bar{t}^2 \\ \varphi_C(\bar{t}) &= \varphi^i_0 + \varphi^i_1\bar{t} + \varphi^i_2\bar{t}^2 \\ \kappa_C(\bar{t}) &= \kappa^i_0 + \kappa^i_1\bar{t} + \kappa^i_2\bar{t}^2 \end{aligned} \tag{3}$$

At the points of conjunction between adjacent segments, constraints on the zero, first, and second order continuity are imposed on the trajectory functions; we force the values of the functions and their first and second derivatives computed in two neighboring segments to be equal at the segment's boundaries.

The proposed approach can also include any direct measurement of the sensor position and attitude with GPS and INS instruments or ephemeris data. These observations may not be optimal for high-precision direct georeferencing. First of all, in case of GPS/INS measurements, the observations refer to the GPS antenna and the INS instrument, not to the sensor perspective center (as required in the collinearity

conditions); the offsets and boresight angles between the GPS, INS, and camera systems, if not known or not accurate enough, should be imported in the collinearity equations, estimated, and removed from the observations. Another important aspect to take into account is that the observations may contain residual systematic errors that were not eliminated in the filtering procedures. For these reasons, the external orientation modeling must be extended in order to integrate and correct the GPS and INS observations. The PPM approach is appropriate for this extension, as already proved in (Grün and Zhang, 2002). The trajectory is again divided into segments; the sensor attitude and position of each image line l belonging to segment i, indicated with $[X_C, Y_C, Z_C, \omega_C, \varphi_C, \kappa_C]_l^i$, are modeled as the sum of the measured position and attitude data for that line $[X_{instr}, Y_{instr}, Z_{instr}, \omega_{instr}, \varphi_{instr}, \kappa_{instr}]_l$ plus the second order polynomial functions depending on $\bar{t}$:

$$\begin{aligned}
X_C(\bar{t}) &= X^i_{instr} + X^i_0 + X^i_1\bar{t} + X^i_2\bar{t}^2 \\
Y_C(\bar{t}) &= Y^i_{instr} + Y^i_0 + Y^i_1\bar{t} + Y^i_2\bar{t}^2 \\
Z_C(\bar{t}) &= Z^i_{instr} + Z^i_0 + Z^i_1\bar{t} + Z^i_2\bar{t}^2 \\
\omega_C(\bar{t}) &= \omega^i_{instr} + \omega^i_0 + \omega^i_1\bar{t} + \omega^i_2\bar{t}^2 \\
\varphi_C(\bar{t}) &= \varphi^i_{instr} + \varphi^i_0 + \varphi^i_1\bar{t} + \varphi^i_2\bar{t}^2 \\
\kappa_C(\bar{t}) &= \kappa^i_{instr} + \kappa^i_0 + \kappa^i_1\bar{t} + \kappa^i_2\bar{t}^2
\end{aligned} \quad . \tag{4}$$

The constant terms $[X_0, Y_0, Z_0, \omega_0, \phi_0, \kappa_0]_i$ compensate for the shifts and angular drifts between the image system and the GPS and INS systems, while the linear and quadratic terms $[X_1, Y_1, Z_1, \omega_1, \varphi_1, \kappa_1]$ and $[X_2, Y_2, Z_2, \omega_2, \varphi_2, \kappa_2]_i$ model the additional systematic errors contained in the GPS and INS measurements. Again, at the points of conjunction between adjacent segments, constraints for the zero, first, and second order continuity are imposed on the trajectory functions. The number of segments is decided for each case study according to the trajectory length and smoothness. In general, for satellite orbits, two segments are sufficient, but for sensors carried on airplane or helicopter, a larger number of segments is recommended, as the trajectory is less smooth.

The degree of the polynomial functions modeling the external orientation can be reduced. In fact, all the PPM parameters are introduced in the model as pseudo-observations with suitable weight (according to their accuracy) and can be fixed to suitable values. An interesting application is that by fixing the second-order parameters to zero, the polynomial degree is reduced to 1 and linear functions, instead of quadratic functions, are obtained. This option allows the modeling of the sensor position and/or attitude in each segment with second- or first-order polynomials, according to the characteristics of the trajectory.

The indirect model also includes the improvement of the internal orientation. The self-calibration is used to correct the observations from systematic errors due to the imaging instrument. Among the errors that may occur in the geometry of the CCD arrays and in the optical system, the following ones are taken into account: the displacement of each line in the focal plane, the focal length variation, the symmetric radial and decentering lens distortions, the scale factor in CCD line direction, and the CCD line rotation in the focal plane. They are modeled with suitable functions depending on the so-called additional parameters (APs).

The system is solved with a least-square bundle adjustment, using a suitable number of well-distributed GCPs. The weights for the observations (collinearity, pseudo-observations for the unknowns) are calculated according to the accuracy of the corresponding measurements.

When the bundle adjustment is completed, the internal and external accuracy of the ground coordinates of the observed points are analyzed. For the internal accuracy the sigma naught *a-posteriori* and the planimetric and height precision of the ground coordinates of GCPs and TPs are calculated. For the evaluation of the external accuracy of the adjustment the RMSE of the TPs are computed and compared to their theoretical (expected) values.

Furthermore the significance of the self-calibration parameters is evaluated through their statistical values (mean value and standard deviation). The determinability of the external and internal orientation parameters is decided according to correlations in order to remove any over-parameterization. A blunder detection is also performed with Baarda's data snooping technique.

Once the parameters modeling the internal and external orientation are estimated, it is possible to estimate the ground coordinates of any homologous point measured in the images through forward intersection.

Applications

The sensor model has been used to orient images acquired by airborne and spaceborne pushbroom sensors with different geometric characteristics. As already mentioned in the Introduction, in this paper we report the results achieved with spaceborne sensors.

In order to demonstrate the flexibility of the model, images acquired with single and multi-lens optical systems, synchronous and asynchronous acquisition modes, and different resolutions have been used as reported in Table 1. Among the pushbroom sensors used for photogrammetric applications, the choice of the sensors to use for our tests depended exclusively on their availability. The MOMS-02 dataset was available at our Institute, the MISR and ASTER ones was downloaded at no cost (MISR) and at very low price (ASTER, $55 USD per scene) from NASA, while the EROS-A1 and SPOT-5/HRS images came from external scientific collaborations.

In this section, the results obtained with MOMS-2P, SPOT-5/HRS, and ASTER-VNIR are described. For each sensor the analysis and processing of the data has been carried out following these steps:

1. Analysis of metadata files for the extraction of the acquisition time of each image line, the sensor external and internal orientation (if available), and any additional information on the images.
2. Radiometric preprocessing of the images in order to improve the radiometric quality and facilitate the point measurement.
3. Measurement of object points. The image coordinates are usually estimated with template least-squares matching, while the ground coordinates are given by external providers (i.e., SPOT-5/HRS and EROS-A1 cases), are measured in topographic maps (i.e., MOMS-2P, ASTER, and MISR cases) or in rectified scenes from other sensors (i.e., Landsat).
4. Direct georeferencing of the images. The ground coordinates of the tie points measured in the images are estimated through a forward intersection using the available external and internal orientation. The process accuracy is analyzed

TABLE 1. SENSORS TESTED WITH OUR RIGOROUS SENSOR MODEL

	EROS-A1	SPOT-5/ HRS	ASTER/ VNIR	MOMS-2P	MISR
Preprocessing	x	x	x	x	x
Orientation	x	x	x	x	x
DTM generation		x	x		
GIS applications			x		

through the residuals (RMSE) between the estimated and the correct ground coordinates of the points. In all the case studies reported in this paper, sub-pixel accuracy in the RMSE could not be achieved and the indirect georeferencing approach was used.

5. Indirect georeferencing of the images. A bundle adjustment is performed in order to estimate the ground coordinates of the tie points, the piecewise polynomial model (PPM) parameters for the external orientation and the self-calibration parameters. Different tests are performed varying the number and distribution of GCPs, the PPM parameters (number of segments, degree) and the number of self-calibration parameters. In some cases the tests are limited by the small number of GCPs. The adjustment is evaluated through both the internal accuracy (standard deviation of unit weight *a posteriori*, standard deviation of estimated parameters) and the external accuracy (RMSE of CPs). In order to avoid over-parameterization, the correlation between the unknown parameters, and the significance of the parameters are also analyzed. In addition, the Baarda test is performed to remove blunder observations.

MOMS-2P

The indirect georeferencing model was used to orient a stereo pair acquired by the German MOMS-02, mounted on the Russian MIR station during Priroda mission. The data were provided by DLR. As two lenses acquired the stereo pair, the extensions for multi-lens was used. The values of the additional parameters describing the relative orientation between the lenses were available from the MOMS-2P calibration report (Kornus, 1996), provided by DLR. From the available 29 object points, some of them were used as GCPs and the others as CPs. The parameters used to control the internal accuracy of the adjustment are: the sigma naught *a posteriori* and the sigma of the CPs. The reference system used in the adjustment was the ECR.

The tests were set as follows: (a) external orientation modeling with quadratic functions, varying the number of segments and GCPs, no self-calibration; (b) external orientation modeling with linear and quadratic functions, varying the number of segments and GCPs, no self-calibration; and (c) self-calibration with best external orientation modeling configuration. The sigma naught, sigma and RMSE of CPs obtained by the tests are summarized in Table 2.

As Test 1 addresses, the spacecraft trajectory was divided into 2 and 4 segments (NS = 2 and NS = 4) of the same length; 6 and 10 points were used as GCPs. The corresponding results are reported in the first four rows in Table 2.

In all cases RMSE and sigma of CPs are smaller than 1 pixel. The best RMSE in the CPs, achieved with 10 GCPs and 4 segments, correspond to 0.4, 0.4, and 0.5 pixels in *X*, *Y*, and *Z*, respectively. As expected, by increasing the number of segments, the external orientation functions can better fit the real trajectory, improving the adjustment performance. This is demonstrated by the decrease of the sigma naught *a posteriori* and the sigma of CPs. The difference in the CPs RMSE between 2 segments and 4 segments configurations is less than 0.5 m, corresponding to 3 percent of the ground pixel size. By increasing the number of GCPs, sigma naught *a posteriori* remains approximately constant and the sigma of the CPs decreases, being the system is more stable. Test 2 was performed in order to establish if the polynomial degree of the position or attitude functions could be reduced. Using 6 and 10 GCPs and 2 and 4 segments for the PPM, quadratic functions for the position and linear functions for the attitude (pos = Q, att = L, second group of rows in Table 2) and linear functions for both position and attitude (pos = L, att = L, third group of rows in Table 2) were tested. The comparison between the results achieved with quadratic and linear functions show that, at least with this particular dataset, quadratic functions for both position and attitude are recommended, because they better fit the true trajectory and produce the best results. Finally, a self-calibration was applied using the configuration with 10 GCPs and 17 CPs, 2 and 4 trajectory segments and quadratic external orientation functions (pos = Q, att = Q). The flexibility of the software allows the user to fix any unknown parameters to the desired values with pseudo-observations. Due to the very high correlation between the internal and external orientation for each test with self-calibration, the external orientation parameters were fixed to the values estimated in the same configuration without self-calibration, and only the self-calibration parameters were estimated. In order to determine only the additional parameters (APs) of interest, the tests were repeated with different self-calibration configurations. In the first run, all the self-calibration parameters were freed, and their mean values, sigma, and correlations were analyzed. The unpredictable or correlated parameters were fixed to constant values. The estimated APs were the rotation angle of the CCD line in the focal plane, the radial and decentering distortions for both lenses. Among them, the rotation angle and the second-order radial distortion param-

TABLE 2. RESULTS OBTAINED FROM A MOMS-2P STEREO PAIR USING DIFFERENT GCPS AND CPS CONFIGURATION AND EXTERNAL ORIENTATION MODELING OPTIONS. NS = NUMBER OF SEGMENTS IN PPM, SC = SELF CALIBRATION (Y = YES, N = NO), DEG = DEGREE OF POSITION (=POS) AND ATTITUDE (=ATT) POLYNOMIALS (Q = QUADRATIC, L = LINEAR)

	DEG						RMSE CPs			σ CPs		
NS	pos	att	SC	GCP	CP	$\hat{\sigma}_0$ (μm)	X	Y	Z	X	Y	Z
2	Q	Q	N	6	21	2.7	13.2	8.6	10.0	11.2	8.5	12.0
2	Q	Q	N	10	17	2.7	7.4	7.6	9.1	9.2	6.9	9.9
4	Q	Q	N	6	21	1.5	10.9	7.0	10.2	7.1	5.5	6.3
4	Q	Q	N	10	17	1.6	7.0	7.1	9.6	5.8	4.4	6.1
2	Q	L	N	6	21	3.0	10.9	9.5	12.9	12.0	9.2	12.7
2	Q	L	N	10	17	2.9	7.7	7.9	9.7	10.0	7.5	10.1
4	Q	L	N	6	21	1.8	11.7	7.0	10.7	7.5	6.0	7.9
4	Q	L	N	10	17	1.9	7.2	7.2	10.3	6.4	4.9	6.9
2	L	L	N	6	21	4.1	19.6	7.7	40.8	15.6	11.9	16.8
2	L	L	N	10	17	4.4	14.5	7.4	16.3	28.6	11.1	16.3
4	L	L	N	6	21	2.8	16.2	7.1	34.1	11.1	8.4	12.0
4	L	L	N	10	17	3.1	11.0	7.2	20.6	10.6	7.8	11.4
2	Q	Q	Y	10	17	1.6	6.9	7.5	9.5	5.2	3.7	5.3
4	Q	Q	Y	10	17	1.2	6.8	7.0	9.8	4.2	3.1	4.7

eter results were insignificant. The maximum effect of the other parameters for both lenses is computed for the pixels on the border (u = 1488). The maximum values are for p_1: Δx = 0.010 mm (1 pixel), for p_2: Δy = 0.010 mm (1 pixel) and for k_1: Δy = 0.020 mm (2 pixels). Comparing the values in Table 2 corresponding to NS = 2 and NS = 4, pos = Q, att = Q, GCP = 10, CP = 17, without (SC = N) and with self-calibration (SC = Y), it can be observed that using self-calibration the system converges easier to the solution: the sigma *a posteriori* of the full adjustment reduces considerably together with the sigma of the CPs. The RMSE differs few centimeters, with smaller values in X and Y and larger values in Z (maximum 40 cm). Considering the ground pixel size of 18.0 m, these RMSE differences are not significant. The final RMSE distribution with self-calibration is shown in Figure 1.

Apart of the tests where both the position and attitude are modeled with quadratic functions, the differences between the RMSE and the standard deviation of the CPs vary between 0.5 m and 4 m. Even if these values represent a small fraction of the pixel size (0.45 pixels), they show that the theoretical (expected) accuracy is slightly better than the achieved one. This fact can be explained with a wrong weight assignment to the image and ground coordinates of the object points. In fact, in our software the same weight is used for all the points. If a point is measured with a different accuracy, it may negatively affect the adjustment process.

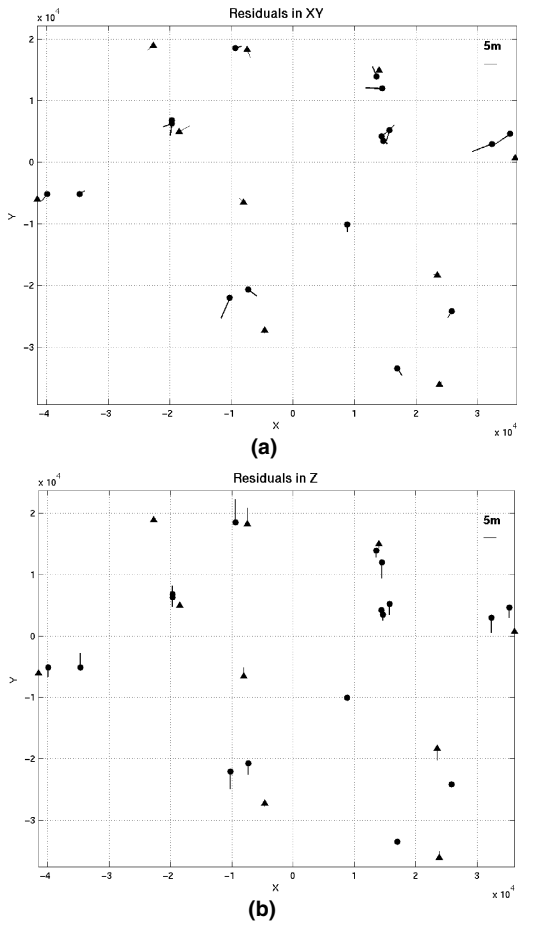

Figure 1. Residuals distributions for MOMS-2P in X, Y (a) and Z (b) using quadratic function for position and attitude (pos = Q, att = Q), NS = 2, 10 GCPs (marked with triangles) and 17 CPs (marked with circles) with self-calibration.

In order to evaluate the performance of our model, the same stereo pair has been oriented using the Spotcheck+ software by Kratky Consulting (Kratky, 1989) mentioned in the Introduction. Using 10 GCPs (the same points used in our tests) and modeling the attitude with quadratic functions, the sigma naught *a posteriori* was 2.2 μm and the residuals achieved in 19 CPs were 5.2 m in East, 4.4 m in North and 11.1 m in height in the Gauss-Krüger coordinate system. The corresponding values achieved with our model in Gauss-Krüger system are 5.5 m, 4.3 m and 11.3 m for East, North, and height, respectively. The results obtained by the two models are very similar; taking into account the ground resolution (18 m), the differences are not significant. In both cases the modeling of the attitude with quadratic functions gave better results, and the correction of the internal orientation parameters (in particular, the focal length and principal point position) using the laboratory calibration or the self-calibration, is recommended.

SPOT-5/HRS

In 2003, the Institute of Geodesy and Photogrammetry (IGP), ETH Zurich, joined the HRS Scientific Assessment Program (HRS-SAP), organized by CNES and ISPRS. This initiative, announced in Denver in 2002 at the ISPRS Commission I Symposium and concluded in Istanbul at the XXth ISPRS Congress, was organized to investigate the potential of the SPOT-5/HRS sensor for DEM generation, in order to help CNES to improve its future Earth Observation systems and all users to better know and trust the accuracy and quality of the HRS instrument and the derived DEM. IGP joined the Initiative as co-investigator and processed the dataset Number 9, over the Chiemsee Lake, in Germany. For more information about the Initiative, see Baudoin *et al.* (2004).

This dataset contained: two stereo images from SPOT5-HRS sensor with corresponding metadata files, the description of the exact position of 81 object points in Germany measured with surveying methods, and seven reference DEMs produced by a different method. The two stereo images were acquired on 01 October 2002 in the morning over an area of approximately 120 km $\times$ 60 km in Bavaria and Austria. Each image is 12,000 pixels $\times$ 12,000 pixels, with a ground resolution of 10 m across and 5 m along the flight (parallax) direction. The scenes were acquired in panchromatic mode in stereo viewing along the flight direction with a base over height ratio of 0.8. The two telescopes contained in the HRS instrument scan the ground with off-nadir angles of +20° (forward image) and −20° (backward image). Each telescope has a 580 mm focal length and a focal plane with a CCD line of 12,000 detectors, 6.5 μm size. The scenes are could free and cover an area with flat, hilly, and mountainous (Alps) terrain, rural zones, towns, rivers, and lakes. The height ranges between 400 m and 2,000 m.

The direct georeferencing approach was used in order to test if the camera calibration and the ephemeris available in the metadata files were accurate enough for high precision mapping. The information on the internal orientation was given through the viewing angles of each detector expressed within the sensor coordinate frame. From these data, the location of each detector in the focal plane was computed. The position and velocity vectors determined by the on-board Doppler Orbitography and Radiopositioning Integrated by Satellite (DORIS) positioning instrument were used for the estimation of the sensor attitude in the ECR system. Then, the position and attitude were interpolated with cubic splines for the acquisition times of the image lines. A forward intersection was applied to calculate the ground

TABLE 3. RESULTS OBTAINED FROM A SPOT-5/HRS STEREO PAIR USING DIFFERENT GCPS AND CPS CONFIGURATION AND EXTERNAL ORIENTATION MODELING OPTIONS. X, Y AND Z REFER TO ECR SYSTEM. NS = NUMBER OF SEGMENTS IN PPM, SC = SELF CALIBRATION (Y = YES, N = NO)

					RMSE CPs (m)			σ CPs (m)		
NS	SC	GCP	CP	$\hat{\sigma}_0$ (μm)	X	Y	Z	X	Y	Z
2	N	6	35	2.7	5.6	8.7	9.4	5.2	8.5	3.7
2	N	12	29	2.9	5.5	7.2	9.2	4.0	7.2	3.1
4	N	6	35	2.6	5.5	8.5	9.2	5.2	8.4	3.6
4	N	12	29	2.8	5.4	7.1	9.0	4.0	7.2	3.1
2	Y	6	35	1.1	3.8	6.9	3.9	2.2	3.2	3.5
2	Y	12	29	1.2	3.7	6.1	3.5	1.7	2.4	2.6
4	Y	6	35	0.8	3.9	6.8	3.7	1.9	2.9	2.8
4	Y	12	29	0.9	3.7	6.0	3.3	1.5	2.3	2.5

coordinates of the object points. The resulting coordinates were compared to the correct values and the RMSE were evaluated. The results showed a large systematic error both in planimetry (2 to 3 pixels) and in height (approximately 3 pixels). Therefore, the indirect georeferencing model was required for the internal and external orientation refinement. From the available 41 points, a group of them was used as GCPs and the remaining as CPs. The *a priori* standard deviation of the GCPs was 3 m. The tests have been carried out with different input configurations as in the case of MOMS-02 dataset.

As already encountered with MOMS-02, the PPM gave better results with quadratic functions, than with linear ones. Using linear functions, the RMS and standard deviation values were close to one pixel. The RMSE and the sigma of the CPs and the sigma naught of the adjustment obtained with quadratic functions without and with self-calibration are reported in Table 3. Taking into account the results achieved without self-calibration (first four rows of Table 3), it can be seen that increasing the number of PPM segments the adjustment converges better (smaller sigma naught a posteriori and sigma of the CPs) and the RMS values remain quite constant. As expected, the use of more GCPs gives better solutions, in terms of internal and external accuracy. The RMSE sizes and distributions in the object space are evidence that if only the external orientation is modeled, the systematic errors are not completely removed. Using self-calibration (last four rows of Table 3 with SC = Y), an improvement both in the internal and external accuracy is seen.

The significant self-calibration parameters were the symmetric radial distortion (through k_1) and the scale in y direction, with the focal length fixed. These parameters were different for each lens and their effect could not be compensated during the estimation of the external orientation parameters only, which is unique for the entire system. The maximum effects of the estimated parameters for each lens are calculated for the pixels on the image borders ($u = \pm 6{,}000$) for k_1 and s_y. They are reported in Table 4.

TABLE 4. MAXIMUM ERRORS IN LENSES 1 (FORWARD) AND 2 (BACKWARD) CAUSED BY LENS DISTORTION. THE ERRORS ARE EXPRESSED IN MM AND IN PIXELS: κ_1: RADIAL DISTORTION, s_y: SCALE IN CCD LINE DIRECTION

	Lens 1	Lens 2	Δy_1 (mm)	Δy_2 (mm)	Δy_1 (pixel)	Δy_2 (pixel)
k_1	$-5.7 \bullet 10^{-7}$	$-7.7 \bullet 10^{-7}$	−0.020	−0.030	3.6	5.3
s_y	$-5.1 \bullet 10^{-4}$	$-4.8 \bullet 10^{-4}$	−0.020	−0.020	3.6	3.6

The orientation of SPOT-5/HRS stereo scenes has also been investigated in many other research institutes that were involved in the HRS-SAP. The results achieved for the dataset Number 9 are reported and compared to the performances of our model. At the Institute of Geodesy and Photogrammetry another approach based on Rational Polynomial Coefficients (RPC) was used to orient the images. This algorithm is implemented in the SAT-PP software, developed at IGP (Grün *et al.*, 2005). In case of SPOT-5/HRS the images were orientated with four GCPs, with residuals of 5.6 m, 4.0 m, and 2.4 m in East, North, and height, respectively (Gauss-Krüger system). The RMSE obtained with our rigorous model in the Gauss-Krüger system are: 5.9 m, 4.2 m, and 3.5 m shown in Figure 2. The differences between the two methods are not very significant. It must be taken into account that, in general, the rigorous models are sensitive to the GCPs distribution in the images, and in our case, the GCPs were located in the left part of the image only. On the other hand, the RPC were derived from the strict model designed for the full scene and the use of a block adjustment could compensate additional systematic errors. The differences in the orientation performance are of course present in the DSMs also, with values in the order of 5 percent of the pixel.

More than 30 publications on the orientation of HRS scenes within the HRS-SAP are available in the Proceedings of the XXth Congress of the International Society for Photogrammetry and Remote Sensing in Istanbul, Turkey in July 2004. Among them, we can mention (Jacobsen, 2004; Toutin *et al.*, 2004; Reinartz *et al.*, 2004; Michalis and Dowman, 2004). In particular, the DEMs obtained by the HRS-SAP principal investigators and the co-investigators over the test area Number 9 were compared with the same strategy and reported in (Rudowski, 2004). In this analysis the DEMs generated at IGP using our sensor model and the RPC model (Poli *et al.*, 2004) and two others have been evaluated through the 2.5D height difference with the reference terrain models, produced with laser scanner (height accuracy = 0.5 m), contour lines (height accuracy = 5.0 m), or photogrammetric methods (height accuracy = 2.0 m). The best mean and RMSE values for 98 percent of the compared points were achieved in about all the reference areas by P1 and P2. The differences between P1 and P2 have already been documented. The mean values obtained with our model were in the range (2.9 m to 4.1 m) in flat and hilly terrain, up to 6.7 m in mountainous areas. The RMSE was in the range (2.8 m to 4.3 m) in flat and hilly terrain, and up to 7.9 m in mountainous areas. This comparison confirms that for this dataset our sensor model can achieve an accuracy both in the CPs and in the interpolated points in the same order or even better than the one obtained using other software and approaches.

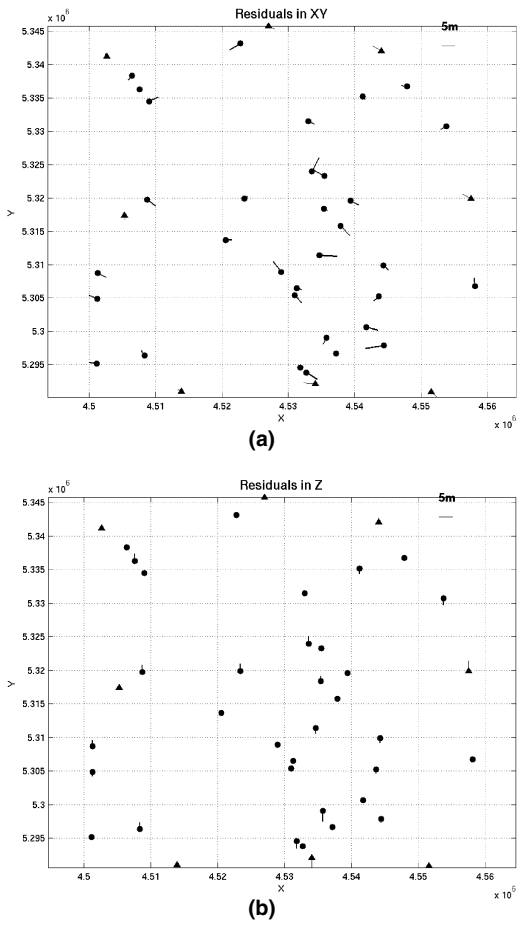

Figure 2. Residuals in planimetry (a) and height (b) for SPOT-5/HRS in Gauss-Krüger system for all object points in the configuration with two segments in the PPM and eight GCPs (marked with triangles) with self-calibration.

ASTER

The Advanced Spaceborne Thermal Emission and Reflection Radiometer (ASTER) is one of the instruments flying on the NASA's Earth Observing System (EOS). The ASTER instrument consists of three downlooking sub-systems: the Visible and Near-infrared (VNIR), the ShortWave Infrared (SWIR), and the Thermal InfraRed (TIR). The instrument used for the DEM generation is the VNIR, the only one with stereo capability. It consists of two independent telescopes looking nadir (channels 1, 2, and 3N) and backward (channel 3B), with an angle of 27.6°. Channels 3N and 3B acquire in the same spectral range (infrared). The CCD lines for each band consist of 5,000 detectors, but not all of them are active at one time. The detector pixel size is different in the two telescopes. In the nadir one, the size is 7.0 μm $\times$ 7.0 μm, while in the backward one it is 6.1 μm $\times$ 6.1 μm. The ASTER scenes are available at different processing levels, as described in (Abrams and Hook, 2002). For our purposes, level 1A is used, because it is not georeferenced and reflects the original acquisition geometry. The scenes were acquired on 25 June 2003 in the morning over Switzerland (orbit 18714, path 195, row 27). They cover an area of approximately 60 km $\times$ 60 km.

The stereo pair formed by the 3N and 3B images has been oriented using the indirect georeferencing model. The software has been adapted in order to treat stereo images, such as these, with different size and CCD detector dimensions. For the orientation, the same procedure used for MOMS-2P and SPOT-5/HRS has been followed. For each test the internal and external accuracy of the system have been analyzed through the sigma naught *a posteriori*, the standard deviation and the RMSE of the CPs. Using the blunder detection included in the model with a threshold of 3.0 (critical value of the t-Student distribution with infinite redundancy and a confidence interval of 99.9 percent), eight points have been identified as outliers and eliminated. After the blunder removal, the indirect georeferencing model was re-applied. The RMSE of the CPs showed errors in the order of 1 to 2 pixels for almost all configurations, with theoretic values (sigma) of about one pixel and sigma naught a posteriori of 3.5 μm to 3.7 μm. The bundle adjustment was repeated with self-calibration, fixing the external orientation to the values previously estimated without self-calibration and keeping the APs free. Different tests have been run to check the correlation between the APs and the ground coordinates of CPs, and decide which parameters had to be estimated. From this analysis, the most significant parameters were the radial and decentering distortion and the scale in the CCD line direction. The maximum combined effect of these parameters (evaluated at the extremes of the image lines) was about 14 μm (2.0 pixels) for 3N and 13 μm (2.1 pixels) for 3B. As expected, the correction of the internal orientation parameters improved the internal and external accuracy of the adjustment. The results obtained with four segments in the PPM, with eight and 12 GCPs and with/without self-calibration are reported in Table 5. The distribution of the residuals is shown in Figure 3. These results confirm that for this dataset, the self-calibration was required in order to model more accurately the acquisition geometry of the ASTER scenes. After the orientation, a 3D point cloud has been produced using the estimated parameters for the sensor internal and external orientation and about 1,800,000 points matched with least-squares matching. The accuracy of the resulting point cloud has been evaluated comparing the 3D distance between each point of the measured point cloud and the surface generated from the DHM25 product by Swisstopo (1 to 3 m accuracy). For the analyzed test sites (six blocks with size 17.5 km $\times$ 12.0 km), the mean values are smaller than one pixel, while the RMSE and standard deviations are slightly larger than one pixel. The effect of the trees, which was proved with further analysis, was not removed. The results achieved in the image orientation and in the DEM accuracy are within the specifications of the absolute DEM product (5 to 15 m for the RMSE of GCPs, 7 to 30 m for the DEM (Hirano *et al.*, 2003), and in accordance with the results obtained by other authors. In Toutin and Cheng (2001) an ASTER stereo pair over Drum Mountains, U.S. was orientated using PCI Geomatica OrthoEngine® software and eight GCPs. The residuals in six CPs were 15.8 m, 10.5 m, and 7.9 m. The corresponding DEM was generated and compared with an USGS 7.5-Minute DEM (30 m grid spacing), with a 7.5 m RMS error. The elevation difference had a minimum value of –109 m, a maximum value of 155 m, a mean value of 1.9 m, and a standard deviation of 11.5 m with an 85 percent level of coincidence. In Hirano *et al.* (2003) four ASTER stereo-scenes located in different mountainous areas have been used for DEM generation with R-WEL DMS® software, using from 5 to 12 GCPs. The RMSE in height in the CPs was between 7.3 m and 26.3 m.

TABLE 5. RESULTS OBTAINED FROM AN ASTER/VNIR STEREO PAIR USING DIFFERENT GCPS AND CPS CONFIGURATION AND EXTERNAL ORIENTATION MODELING OPTIONS. X, Y AND Z REFER TO ECR SYSTEM. NS = NUMBER OF SEGMENTS IN PPM, SC = SELF CALIBRATION (Y = YES, N = NO)

					RMSE CPs (m)			σ CPs (m)		
NS	SC	GCP	CP	$\hat{\sigma}_0$ (μm)	X	Y	Z	X	Y	Z
4	N	8	30	3.7	27.6	30.1	22.3	15.2	10.4	14.6
4	N	12	26	3.5	22.6	20.1	16.3	11.2	9.4	8.6
4	Y	8	30	1.1	13.6	14.8	14.4	7.0	3.5	5.8
4	Y	12	26	1.0	12.7	12.2	14.0	6.5	3.4	5.0

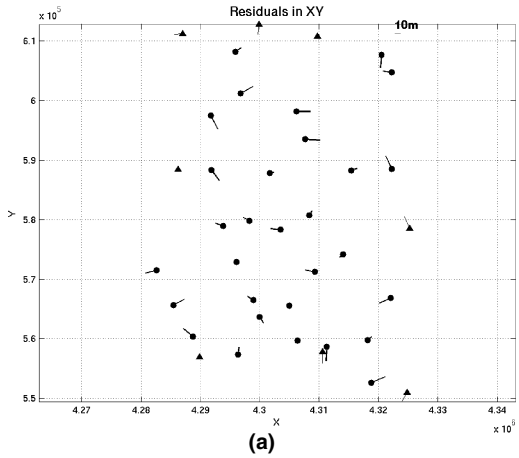

Figure 3. RMSE in planimetry (a) and height (b) for ASTER-VNIR for all object points in the configuration with four segments in the PPM, eight GCPs (marked with triangles) and self-calibration.

Conclusions

In this paper, a rigorous model for their orientation of pushbroom sensors has been presented. The imagery acquired by these sensors have very high potential for photogrammetric mapping at different scales from airborne and satellite platforms, and its orientation is a fundamental step in the processing chain for the generation of orthoimages and Digital Elevation Models (DEMs). The proposed model includes two different orientation approaches. In the direct georeferencing model, the ground coordinates of the homologous points measured in the images are estimated through a forward intersection, using as external orientation the data provided by geopositioning systems carried on board (GPS, INS, star trackers) or the trajectory calculated by mathematical formulas describing the sensor trajectory (only for satellite-based sensors). The alternative orientation method is a self-calibrating bundle adjustment, modified according to the pushbroom sensors' characteristics. If GPS and INS are available, they are integrated in the PPM. The parameters modeling the internal and external orientation, together with the ground coordinates of the tie points, are estimated through a least-squares bundle adjustment using well-distributed ground control points. The use of pseudo-observations allows the user to run the adjustment fixing any unknown parameters to certain values. A blunder detection procedure is integrated for the automatic detection of wrong image coordinate measurements. The false measurements removal is manual.

Thanks to this approach, the resulting model has the advantage of being is very flexible, and therefore can be used for a large number of pushbroom sensors, carried on airborne and spaceborne platforms. In order to demonstrate this, the model was tested with pushbroom sensors different characteristics (single-lens and multi-lens optical systems, various number of linear arrays, synchronous and asynchronous acquisition modes), carried on satellite and helicopter platforms. The results achieved with airborne sensors are described in Poli (2002). In this paper, the results obtained with MOMS-2P, SPOT-5/HRS, and ASTER have been reported. Additional tests with asynchronous sensors (EROS-A1) are in Giulio-Tonolo and Poli (2003).

For each test both the direct and indirect models have been used, and in all cases the direct georeferencing was not accurate enough for high accurate mapping. The indirect model has been applied with different ground control point distributions, varying the PPM configurations (number of segments, polynomials degree) and with and without self-calibration. All the imagery has been oriented with sub-pixels accuracy in the checkpoints using a minimum number of six ground control points. Further investigation could be carried out on the selection of the additional parameters in an automatic way with suitable tests after each iteration.

References

Abrams, M., and S. Hook, 2002. ASTER User HandBook, URL: *http://asterweb.jpl.nasa.gov/documents/aster_user_guide_v2.pdf* (last date accessed: 15 November 2006).

Baltsavias E.P., and D. Stallmann, 1992. Metric information extraction from SPOT images and the role of polynomial mapping functions, *International Archives of Photogrammetry and Remote Sensing*, Vol. 29, Part B4, Washington D.C., pp. 358–364.

Baltsavias, E.P., and D. Stallmann, 1996. Geometric potential of MOMS-02/D2 data for point posi-tioning, DTM and orthoimage,

International Archives of Photogrammetry and Remote Sensing, Vol. 31, Part B4, Vienna, Austria, pp. 110–116.

Baudoin, A., M. Schroeder, C. Valorge, M. Bernard, and V. Rudowski, 2004. The HRS-SAR Initiative: A scientific assessment of the high resolution stereoscopic instrument on board of SPOT 5 by ISPRS investigators, *International Archives of Photogrammetry and Remote Sensing*, Vol. 35, Part B1, Istanbul, Turkey, pp. 372–378.

Büyüksalih, G., and K. Jacobsen, 2000. Geometric aspects of MOMS-2P three-line imagery for mapping applications, *Proceedings of Annual Meeting of the Remote Sensing Society*, Lancaster, UK.

Dowman, I.J., and P. Michalis, 2003. Generic rigorous model for along track stereo satellite sensors, *Proceedings of ISPRS Workshop – High Resolution Mapping from Space 2003*, 04–06 October, Hannover, unpaginated CD-ROM.

Ebner, H., W. Kornus, and T. Ohlhof, 1992. A simulation study on point determination for the MOMS-02/D2 space project using an extended functional model, *International Archives of Photogrammetry and Remote Sensing*, Vol. 29, Part B4, Washington D.C., pp. 458–464.

Fritsch, D., and D. Stallmann, 2000. Rigorous photogrammetric modelling processing of high resolution satellite imagery, *International Archives of Photogrammetry and Remote Sensing*, Vol. 33, Part B1, Amsterdam, pp. 313–321.

Giulio-Tonolo, F., and D. Poli, 2003. Georeferencing of EROS-A1 high resolution images with rigorous and rational function model, *Proceedings of ISPRS Workshop – High Resolution Mapping from Space 2003*, October 2003, Hannover, unpaginated CD-ROM.

Grün, A., and L. Zhang, 2002. Automatic DTM generation from three-line-scanner (TLS) images, *International Archives of Photogrammetry and Remote Sensing*, Vol. 34, Part 2A, Graz, Austria, pp. 131–137.

Grün, A., F. Remondino, and L. Zhang, 2004. The Bamiyan valley: Landscape modelling for cultural heritage visualization and documentation, *International Archives of Photogrammetry and Remote Sensing*, Vol. 36. Part 5/W1, unpaginated CD-ROM.

Grün, A., L. Zhang, and H. Eisenbeiss, 2005. 3D precision processing of high-resolution satellite imagery, *Proceedings of ASPRS Annual Meeting 2005*, Baltimore, Maryland, 07–11 March, unpaginated CD-ROM.

Gugan, D.J., and I.J. Dowman, 1988. Accuracy and completeness of topographic mapping from SPOT imagery, *The Photogrammetric Record*, 72(12):787–796.

Hirano, A., R. Welch, and H. Lang, 2003. Mapping from ASTER stereo image data: DEM validation and accuracy assessment, *ISPRS Journal of Photogrammetry and Remote Sensing*, 57:356–370.

Hofmann, O., P. Navé, and H. Ebner, 1982. DPS – A digital photogrammetric system for producing digital elevation models and orthophotos by means of linear array scanner imagery, *International Archives of Photogrammetry and Remote Sensing*, Vol. 24, Part 3, Helsinki, Finland, pp. 216–227.

Jacobsen, K., G. Konecny, and H. Wegmann, 1999. High resolution sensor test comparison with SPOT, KFA1000, KVR1000, IRS-1C and DPA in lower Saxony, *International Archives of Photogrammetry and Remote Sensing*, Vol.32, Part 4, Stuttgart, Germany, pp. 260–269.

Jacobsen, K., and R. Passini, 2003. Accuracy of digital orthophotos from high resolution space imagery, *Proceedings of ISPRS Workshop – High Resolution Mapping from Space 2003*, 04–06 October, Hannover, Germany, unpaginated CD-ROM.

Jacobsen, K. 2004. DEM generation by SPOT HRSC, *International Archives of Photogrammetry and Remote Sensing*, Vol. 35, Part B1, Istanbul, Turkey, pp. 439–444.

Konecny, G., P. Lohmann, H. Engel, and E. Kruck, 1987. Evaluation of SPOT imagery on analytical photogrammetric instrument, *Photogrammetric Engineering & Remote Sensing*, 53(9):1223–1230.

Kornus, W., 1996. *MOMS-2P Geometric Calibration Report: Results of Laboratory Calibration (Version 1.1)*, DLR, Institute of Optoelectronic, November.

Kornus, W., M. Lehner, and M. Schoeder, 1999. Photogrammetric block adjustment using MOMS-2P imagery of the three intersecting stereo-strips, *Proceedings of ISPRS Workshop - Integrated Sensor Calibration and Orientation*, Portland, Maine, 16–17 June.

Kratky, V., 1989. Rigorous photogrammetric processing of SPOT images at CCM Canada, *ISPRS Journal of Photogrammetry and Remote Sensing*, 44:53–71.

Image, 2005. URL: *http://image.gsfc.nasa.gov* (last date accessed: 15 November 2006).

Michalis, P., and I. Dowman, 2004. A rigorous model and DEM generation for Spot5/HRS, *International Archives of Photogrammetry and Remote Sensing*, Vol. 35, Part B1, Istanbul, Turkey, pp. 410–415.

Olhof, T., and W. Kornus, 1994. Geometric calibration of digital three-line CCD cameras, *International Archives of Photogrammetry and Remote Sensing*, Vol. 30, Part 1, Como, Italy, pp. 71–81.

Olhof, T., 1995. Block triangulation using three-line images, *Proceedings of Photogrammetric Week 1995* (Wichmann Verlag, editor), Stuttgart, pp. 197–206.

Poli, D., G. Seiz, and E.P. Baltsavias, 2000. Cloud-top height estimation from satellite stereopairs for weather forecasting and climate change analysis, *International Archives of Photogrammetry and Remote Sensing*, Vol. 33, Part B7/3, Amsterdam, The Netherlands, pp. 1162–1169.

Poli, D., 2002. General model for airborne and spaceborne linear array sensors, *International Archives of Photogrammetry and Remote Sensing*, Vol. 34, Part B1, Denver, Colorado, pp. 177–182.

Poli, D., L. Zhang, and A. Grün, 2004. SPOT-5/HRS stereo images orientation and automated DSM generation, *International Archives of Photogrammetry and Remote Sensing*, Vol. 34, Part B1, Istanbul, Turkey, pp. 421–432.

Poli, D., 2002. General model for airborne and spaceborne linear array sensors, *International Archives of Photogrammetry and Remote Sensing*, Denver, Colorado, Vol. 34, Part B1, pp. 177–182.

Reinartz, P., M. Lehner, R. Mueller, and M. Schroeder, 2004. Accuracy analysis for DEM and orthoimages derived from SPOT-HRS stereo data without using GCP, *International Archives of Photogrammetry and Remote Sensing*, Vol. 34, part B1, Istanbul, pp. 433–438.

Rudowski, V., 2004. Synthesis of studies relating to HRS DTM production, *International Archives of Photogrammetry and Remote Sensing*, Vol. 35, Part B1, Istanbul, pp. 399–409.

Seidelmann, P.K., B. Guinot, and L.E. Dogget, 1992, *Explanatory Supplement to the Astronomical Almanac* (P.K. Seidelmann, editor), U.S. Naval Observatory, University Science Books, Mill Valley, California.

Seiz, G., A. Gruen, S. Tjemkes, and R. Davies, 2004. Multi-view cloud-top height and wind retrieval with photogrammetric methods: Application to Meteosat-8 HRV observations, *Proceedings of 7th International Winds Workshop*, Helsinki, 14–17 June, unpaginated CD-ROM.

SPOT Satellite Geometry Handbook, 2002. *Reference S-NT-73-12-SI*, Edition 1, Revision 0, Date: 2002–01–15.

Toutin, T., and P. Cheng, 2001. DEM generation with ASTER stereo data, *Earth Observation Magazine*, 10:10–13.

Toutin, T., 2004a. Comparison of stereo-extracted DTM from different high-resolution sensors: SPOT-5, EROS-A, IKONOS-II, and Quickbird, *IEEE Transactions on Geoscience and Remote Sensing*, 42(10):2121–2129.

Toutin, T., 2004b. Review Paper: Geometric processing of remote sensing images: Models, algorithms and methods, *International Journal of Remote Sensing*, 25(10):1893–1924.

Toutin, T., P. Briand, and R. Chénier, 2004. DTM generation from SPOT HRS in-track stereo images, *International Archives of Photogrammetry and Remote Sensing*, Vol. 35, Part B1, Istanbul, Turkey pp. 416–420.

Valadan-Zoej, M.J.V., and M.J. Foomani, 1999. Mathematical modelling and geometric accuracy testing of IRS-1C stereo-pairs, *Proceedings of ISPRS Workshop – High Resolution Mapping from Space 2001*, 18–21 September, Hannover, Germany, unpaginated CD-ROM.

(Received 29 June 2005; accepted 06 September 2005; revised 19 October 2005)